Obrabotka metallov (tekhnologiya, oborudovanie, instrumenty) = Metal Working and Material Science. 2026 vol. 28 no. 3 pp. 229–249
ISSN: 1994-6309 (print) / 2541-819X (online)
DOI: 10.17212/1994-6309-2026-28.3-229-249

NSTU NETI

Obrabotka metallov -
Metal Working and Material Science

Journal homepage: http://journals.nstu.ru/obrabotka_metallov

Effect of severe plastic deformation and heat treatment on the structural, mechanical and tribological properties of Cu-9Al-2Mn bronze

Andrey Filippov [a, *], *Nikolay Shamarin* [b], *Sergei Tarasov* [c], *Natalya Semenchuk* [d]

Institute of Strength Physics and Materials Science of the Siberian Branch of the RAS, 2/4, pr. Akademicheskii, Tomsk, 634055, Russian Federation

[a] https://orcid.org/0000-0003-0487-8382, avf@ispms.ru; [b] https://orcid.org/0000-0002-4649-6465, shnn@ispms.ru;
[c] https://orcid.org/0000-0003-0702-7639, tsy@ispms.ru; [d] https://orcid.org/0000-0001-6547-7676, natali.t.v@ispms.ru

ARTICLE INFO

Article history:
Received: 29 June 2026
Revised: 11 July 2026
Accepted: 14 July 2026
Available online: 15 September 2026

Keywords:
Bronze
Microstructure
Phase composition
Mechanical properties
Severe plastic deformation
Scratching
Sliding friction

Funding
The work was carried out under the state assignment for ISPMS SB RAS, project FWRW-2026-0001.

ABSTRACT

Introduction. Severe plastic deformation (*SPD*) is one of the most promising methods for modifying the structure of non-ferrous alloys, enabling them to be transformed into ultrafine-grained (*UFG*) and nanocrystalline states. At the same time, for the practical implementation of such materials in machine-building equipment components, the issues of their thermal stability and wear resistance under extreme loads during contact interaction in scratching and sliding friction remain critically important. ***The purpose of the work*** is a comprehensive study of the effect of various thermal and severe plastic deformation conditions on the structural, mechanical and tribological characteristics of *Cu-9Al-2Mn* bronze. The paper studies samples of *Cu-9Al-2Mn* bronze in different initial states: annealed at 700°C, quenched from 900°C and aged at 400°C. To form a *UFG* structure and enhance strength properties, the workpieces were subjected to deformation processing by multi-axial forging at room temperature followed by rolling. In order to study recrystallization processes and the thermal stability of the *UFG* alloy, annealing was performed at 400°C for 30 minutes and at 500°C for 10 minutes. **Materials and methods.** Metallography, transmission electron microscopy and X-ray diffraction analysis were used as the primary methods for characterizing the structure and phase composition. Mechanical properties were evaluated based on Vickers microhardness measurements and static tensile tests. Resistance to localized surface damage was determined by scratch testing under a linearly increasing load from 0.5 to 30 N. Wear resistance and coefficient of friction were investigated under dry sliding friction using a pin-on-disc scheme (counterbody — steel 52100) under a load of 20 N and at a constant speed of 0.1 m/s. Monitoring of the tribosystem dynamics was carried out using vibrometry and recording acoustic emission (*AE*) signals. The surface topography of wear tracks and balls was studied by confocal laser scanning microscopy. The change in structure beneath the friction surface was also investigated using metallography. **Results and discussion.** The effect of heat treatment, severe plastic deformation (*SPD*), and subsequent annealing on the structure, mechanical, and tribological properties of *Cu-9Al-2Mn* bronze is studied. It is shown that *SPD* (multi-axial forging and rolling) produces an ultrafine-grained (100–300 nm) structure with high dislocation density and deformation martensite, resulting in a yield strength of 998 MPa and a microhardness of 3.24 GPa. Low-temperature annealing at 400°C further increases the yield strength to 1,095 MPa owing to polygonization and precipitation hardening. Annealing at 500°C induces recrystallization, partially restoring ductility. Tribological tests under dry sliding friction revealed that *SPD* significantly enhances wear resistance while maintaining an unchanged coefficient of friction. Scratch depth in scratch testing is reduced by ~40%, and the damage mechanism changes from ductile ploughing to microcutting. Acoustic emission and vibration correlate with the change in wear mechanisms.

For citation: Filippov A.V., Shamarin N.N., Tarasov S.Yu., Semenchuk N.A. Effect of severe plastic deformation and heat treatment on the structural, mechanical and tribological properties of Cu-9Al-2Mn bronze. *Obrabotka metallov (tekhnologiya, oborudovanie, instrumenty) = Metal Working and Material Science*, 2026, vol. 28, no. 3, pp. 229–249. DOI: 10.17212/1994-6309-2026-28.3-229-249. (In Russian).

Introduction

An important task for modern industry is to increase the service life and reliability of machine and mechanism parts. Mechanical surface damage and wear can significantly reduce the service life of a part, leading to its damage and failure of expensive equipment.

Modern scientific and technical data indicate the possibility of significantly improving the physical-mechanical and operational characteristics of materials through controlled changes in their structural state [1]. One of the most effective tools for such control is severe plastic deformation (*SPD*) combined with

*** Corresponding author**
Filippov Andrey V., Ph.D. (Engineering), Head of Laboratory
Institute of Strength Physics and Materials Science
of the Siberian Branch of the RAS,
2/4, pr. Akademicheskii,
634055, Tomsk, Russian Federation
Tel.: +7 999 178-13-40, **e-mail:** avf@ispms.ru

heat treatment, which allows for the targeted modification of submicro- and nanocrystalline structures that possess a unique set of properties [2, 3].

Among structural materials used in sliding friction units, aluminum bronzes [4], particularly *Cu-9Al-2Mn* bronze, hold a special place. Aluminum at a content of ~9% does not completely dissolve in the copper *FCC* lattice and contributes to the formation of the **β**-(Cu_3Al) phase, which serves to enhance the strength and hardness of the alloy.

By using annealing, quenching, and aging, it is possible to significantly influence the phase composition and properties of this alloy [5–7]. Manganese stabilizes the **β**-phase and partially suppresses its decomposition, leading to the formation of the brittle eutectoid phase $\boldsymbol{\gamma_2}$ (Cu_9Al_4). This contributes to maintaining good plasticity of the alloy and opens up the possibility of applying *SPD* methods for structure modification. Additionally, the addition of manganese increases corrosion resistance and promotes the refinement of structural components, making this alloy suitable for the production of sliding bearings, guides, and other wear-prone parts. However, for the effective application of this alloy after modification by *SPD* methods, it is necessary to thoroughly study the relationships between the resulting structure and the final mechanical and tribological properties.

Traditional methods of hardening aluminum bronzes, including quenching and aging, allow for the variation of phase composition and the dispersion of precipitates; however, they do not always ensure a sufficient level of wear resistance. At the same time, repeated severe plastic deformation, implemented through methods of multi-directional forging and subsequent rolling at room temperature, is capable of refining the grains. Subsequent low-temperature annealing allows for the regulation of the balance between strength and plasticity, as well as influencing material properties [8]. This should have a positive effect on hardness, strength, and wear resistance.

The values of the coefficient of friction and wear, measured over a long period, do not always reflect the rapid processes occurring on the worn surface: adhesive bonding, loss of load-bearing capacity due to the destruction of previously formed anti-friction oxide films, or structural evolution. In modern tribology, diagnostic methods based on vibrometry and acoustic emission are used, which have high sensitivity to dynamic changes in the sliding contact zone [9–13]. In this regard, in recent years, the focus of research attention has shifted toward a comprehensive analysis of the dynamic response of tribosystems with the simultaneous use of vibrometry and the acoustic emission (*AE*) method [14–16].

The *AE* method is based on the recording of sound or ultrasonic frequency waves generated by a solid body under load as a result of local microdeformations. In tribological systems, the sources of *AE* are the elastoplastic deformation of microirregularities, the initiation and propagation of subsurface cracks, as well as the adhesive failure of microcontact bridges [13]. Synchronous recording of vibration accelerations complements the picture by recording macroscopic oscillations of the elements of the tribosystem, caused by macro-roughness and frictional instability of the contact.

The purpose of this work is a comprehensive study of the influence of various thermal and severe plastic deformation modes on the structural, mechanical, and tribological characteristics of *Cu-9Al-2Mn* bronze.

To achieve the stated purpose, ***the following tasks*** were addressed in this work:

– to investigate the structure and determine the mechanical properties of samples in different structural states;

– to conduct studies on surface damage during scratching of samples;

– to conduct studies on the tribological properties of samples under unlubricated sliding conditions;

– to investigate the state of the surface of scratches and wear tracks.

Materials and methods

For the purpose of this research, samples with different structural states were fabricated from the *Cu-9Al-2Mn* alloy. The techniques used for preparation and the designation of samples adopted in this work are presented in Table.

For mechanical testing by tension and by indentation, samples were cut using electro-discharge machining, followed by surface grinding of the samples. The samples were subjected to tensile testing using

Sample designation and processing conditions

Sample designation	Structural state formation method
1	Annealing of hot-rolled rods at 700 °C for 3 h
2	Quenching of hot-rolled rods from 900 °C in water
3	Aging of quenched rods at 400 °C for 8 h
4	Multi-directional 3D forging to 40 % plastic strain
5	Rolling after multi-directional forging to 50 % plastic strain
6	Low-temperature annealing (30 min at 400 °C) after rolling, followed by water quenching
7	Low-temperature annealing (10 min at 500 °C) after rolling, followed by water quenching

a *Testsystem UTS-110M* testing machine. The loading speed was 1 mm/min. Microhardness measurements were conducted using a *Tochline-TBM* microhardness tester at a load of 100 N.

To study the structure, metallographic investigations were conducted. The structure of the samples after *SPD* was studied using a transmission electron microscope, the *JEOL JEM-2100*.

The phase composition was studied using a *DRON* diffractometer with a symmetric scheme and *Co-K*α radiation.

To determine the scratch resistance of the samples, a *Revetest RST* scratch tester was used. The scratching speed, length, and load were 10 mm/min, 3 mm, and 0.5–30 N, respectively.

Tribological tests were conducted on a pin-on-disk tribometer with a constant sliding speed of 0.1 m/s and a normal load of 20 N under dry sliding friction. The disks were cut from bronze with different structural states. The counterbodies were *AISI 52100* steel balls, which were securely fixed in a special holder. During sliding, acoustic emission and vibration acceleration signals were recorded using an *EYA-2* setup and an accelerometer with a *NI-9234* data acquisition system, respectively. An *Olympus OLS-4100* confocal laser scanning microscope was used to investigate the surface condition of the samples after friction.

Results and discussion

Based on the analysis of metallographic images, it is evident that after annealing at 700 °C (sample 1), the structure of the bronze is represented by large grains (20–40 μm) of the **α**-*Cu(Al,Mn)* solid solution (Fig. 1,*a*). The polygonal and nearly equiaxed grains indicate that recrystallization occurred at 700 °C, destroying the rolling texture and reducing the density of linear defects. Dark areas are also visible in the image, which are presumably precipitates of the brittle intermetallic γ_2-(Cu_9Al_4) phase, formed as a result of the eutectoid decomposition of the high-temperature $\boldsymbol{\beta}$-$(Cu_3Al) \rightarrow \boldsymbol{\gamma_2}$-$(Cu_9Al_4)$ + **α**-Cu*(Al,Mn)* under slow cooling conditions.

After quenching in water from a temperature of 900 °C (sample 2), the metallographic image (Fig. 1,*b*) shows that martensite $\boldsymbol{\beta}'$-(Cu_3Al) formed in the alloy alongside **α**-*Cu(Al,Mn)*. According to the phase diagram [17, 18], at a temperature of 900 °C, the alloy is in the region of existence of the high-temperature $\boldsymbol{\beta}$-Cu_3Al phase, which forms directly from the melt. After quenching and depending on local conditions, the samples may contain either $\boldsymbol{\beta}'$-(Cu_3Al) martensite or $\boldsymbol{\gamma_2}$-(Cu_9Al_4), which suggests two possible scenarios for the decomposition of the high-temperature **β**-phase: (1) $\boldsymbol{\beta} \rightarrow \boldsymbol{\beta}'$ and (2) $\boldsymbol{\beta} \rightarrow \boldsymbol{\gamma_2}$-$(Cu_9Al_4)$ + **α**-*Cu*.

After aging the quenched samples at 400 °C for 8 hours (sample 3), the metallographic image (Fig. 1,*c*) shows dispersed precipitates in the form of dark spots around the bright grains of **α**-*Cu(Al,Mn)*. Apparently, the growth of $\boldsymbol{\gamma_2}$-(Cu_9Al_4) occurs due to the decomposition of $\boldsymbol{\beta}'$ into elements [19].

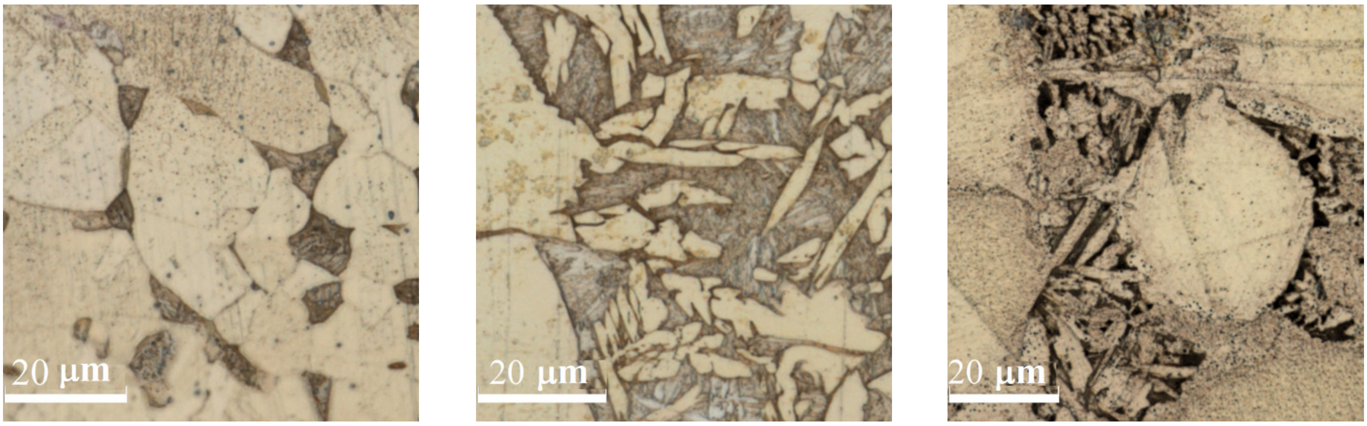

a *b* *c*

Fig. 1. Optical micrographs of the typical microstructure of *Cu-9Al-2Mn* bronze samples. Samples: 1 (*a*), 2 (*b*), 3 (*c*)

According to *TEM* data, a complex structure of deformation-induced martensite was formed in sample 4 (Fig. 2,*a*) after multi-axial forging. The martensitic phase is represented in the form of packets and colonies of parallel submicron-sized laths and needles. Severe plastic deformation led to the complete restructuring of the initial *BCC* matrix (β'-phase) via a shear mechanism and the accumulation of a high density of dislocations [20, 21], resulting in the formation of 18*R* β_1' martensite. Alongside the martensitic transformation, intensive deformation twinning was observed [22]. As a result, alternating laths of β_1' martensite with a width of 50–150 nm and clear flat boundaries were formed [23], within which nanoscale microtwins are discernible. The change in loading axis during deformation activated the development of intersecting twinning systems, leading to structural grain subdivision, effective grain refinement to an ultrafine-grained state, and contributed to significant strain hardening of the material.

Additional plastic deformation by rolling (sample 5, Fig. 2,*b*) led to the formation of a characteristic intersecting band morphology, creating a network substructure. Deformation of 18*R* martensite can lead to its reorientation and the emergence of new variants, while during unloading it may exhibit pseudoelasticity. Despite the relative stability of β_1' martensite under severe plastic deformation, the original martensite plates ultimately underwent segmentation. As a result of this process, the martensite laths broke into isolated nanosized subgrains and rectangular blocks with characteristic dimensions in the range of 100 to 300 nm. In certain areas of the material, a high density of dislocations was observed. At the same time, microtwins within the martensitic laths were preserved. This, in turn, suggests an even more significant increase in the strength of the alloy due to the barrier effect of numerous interphase and interblock boundaries.

Subsequent annealing after rolling at 400 °C for 30 minutes (sample 6) led to the activation of recovery and polygonization processes (Fig. 2,*c*). The *TEM* image shows a significant reduction in the density of nonequilibrium lattice defects and the relaxation of internal stresses caused by rolling. The transformation of martensitic laths into a grain-subgrain structure with clearly defined low-angle boundaries and a small proportion of high-angle boundaries was observed. Along the subboundaries and at the triple junction nodes, the appearance of local dark contrast was noted, indicating the initial stages of recrystallization and the formation of fine-dispersed excess phases. At the same time, elements of the original lath morphology were partially inherited, forming a submicron structure of a mixed type.

Increasing the temperature during short-term annealing to 500 °C (sample 7) after rolling led to a change in the mechanism of structural changes and the development of intense recrystallization (Fig. 2,*d*). In the *TEM* image, the complete disappearance of the lath and cellular morphology is visible. The structure was transformed into a submicron one with a bimodal grain size distribution, with sizes ranging from 300 to 700 nm. Most of the formed grains are characterized by an internal structure free from dislocation clusters and by the presence of clearly defined flat high-angle boundaries with equilibrium angles at triple junctions.

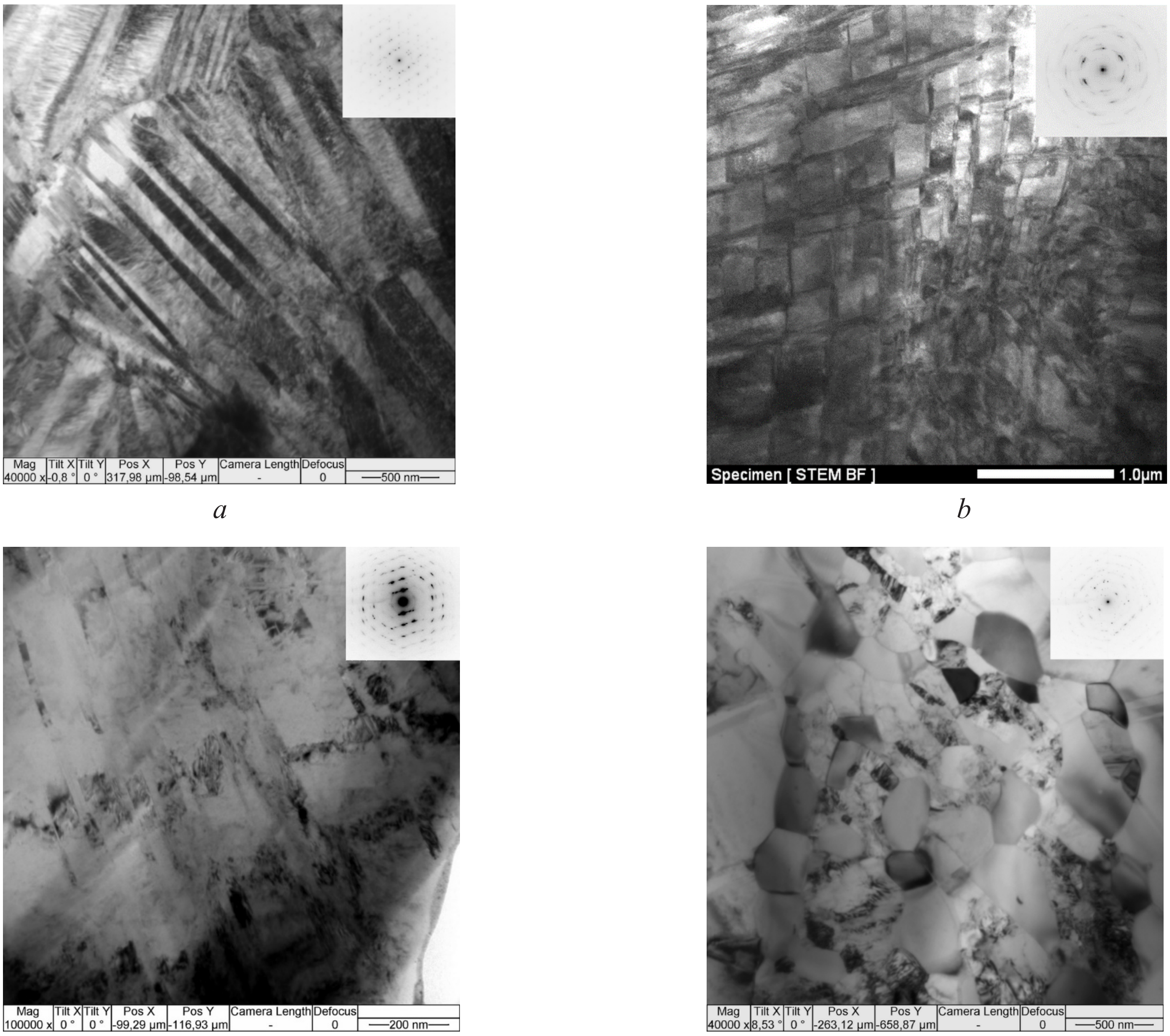

a *b*

c *d*

Fig. 2. TEM images of the typical microstructure of *Cu-9Al-2Mn* bronze samples: samples 4 (*a*), 5 (*b*), 6 (*c*), and 7 (*d*)

The structure shows annealing twin boundaries, indicating the completion of primary recrystallization. At the same time, dispersed grain-subgrain structures with residual dislocation density were observed in local volumes of the material, indicating the incompleteness of recrystallization in the volume.

Based on X-ray diffraction, the phase composition of the studied bronze samples was investigated. After annealing the hot-rolled rod at 700 °C (sample 1, Fig. 3,*a*), in addition to the intense reflections of the **α**-*Cu(Al,Mn)* solid solution (*FCC* lattice), a set of additional peaks characteristic of the γ_2-(Cu_9Al_4) and **β′**-(Cu_3Al) phases is present.

Rapid cooling during quenching (sample 2, Fig. 3,*b*) apparently does not prevent the eutectoid transformation β → γ_2-(Cu_9Al_4) + **α**-*Cu(Al,Mn)*, since, along with the peaks of **β′**-Cu_3Al, the peaks of γ_2-(Cu_9Al_4) are also present. This situation may be due to the small stabilizing effect of the addition of 2 wt.% manganese on the **β** phase. Thus, X-ray diffraction confirms the previously made conclusion about the dual nature of the decomposition of the high-temperature **β**-phase in this alloy.

After aging at 400 °C (sample 3, Fig. 3,*c*), processes of diffusion phase decomposition are initiated. The X-ray diffraction pattern shows a clear increase in intensity and the appearance of new reflections belonging to the intermetallic γ_2-phase. This fact indicates the progression of the aging process according to the scheme of residual martensite decomposition with the formation of the eutectoid components. At the same time, there is a broadening and decrease in the intensity of the martensitic phase peaks, which confirms its thermal decomposition.

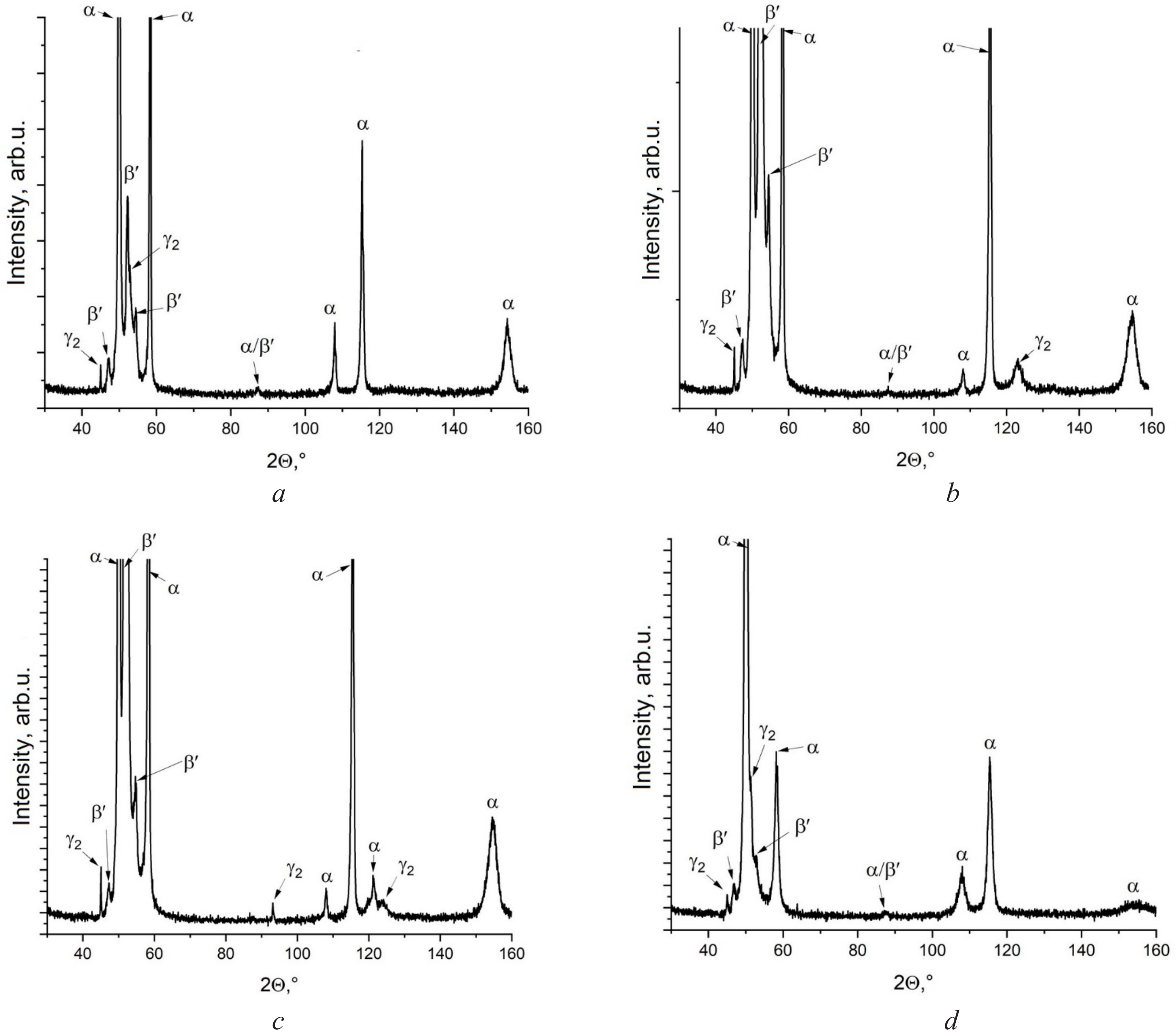

Fig. 3. X-ray diffraction patterns of samples 1 (*a*), 2 (*b*), 3 (*c*), and 4–7 (*d*)

To describe the samples after *SPD* (multi-axial forging and rolling), one characteristic X-ray diffraction pattern obtained for the sample after rolling (Fig. 3,*d*) was selected. This diffraction pattern shows a significant change in the shape of the diffraction peaks. The main reflections of the **α**-phase and deformation-induced $\boldsymbol{\beta}_1'$ martensite broaden, and their intensity decreases. Such a diffraction profile is characteristic of the formation of an ultrafine-grained structure.

To determine the influence of the structural-phase state on the mechanical properties of the studied bronze samples, tensile tests were conducted (Fig. 4,*a*) and their microhardness was measured (Fig. 4,*b*). After annealing at 700 °C (sample 1), the bronze is characterized by minimal microhardness and strength. But at the same time, it is the most ductile. Rapid cooling in water from 900 °C (sample 2) leads to a significant increase in microhardness to 2.42 GPa and tensile strength to 779 MPa, while plasticity decreases by more than twofold (21.4%). After aging at 400 °C (sample 3), the properties returned to a plastic state (47.4%) with ultimate tensile strength ($\boldsymbol{\sigma}_u$ = 631 MPa).

Multiaxial forging (sample 4) led to significant hardening of the material. Microhardness increased to 2.7 GPa, and the yield strength increased by approximately 2.5 times ($\boldsymbol{\sigma}_{0.2}$ = 579 MPa) compared to the annealed state. Rolling after forging (sample 5) provides maximum strengthening of the material. Microhardness reached 3.24 GPa, ultimate tensile strength $\boldsymbol{\sigma}_u$ = 1,130 MPa, yield strength $\boldsymbol{\sigma}_{0.2}$ = 998 MPa. During subsequent annealing at a temperature of 400 °C for 30 minutes (sample 6), despite the thermal treatment, the strength characteristics do not decrease, and the yield strength even slightly increases to its

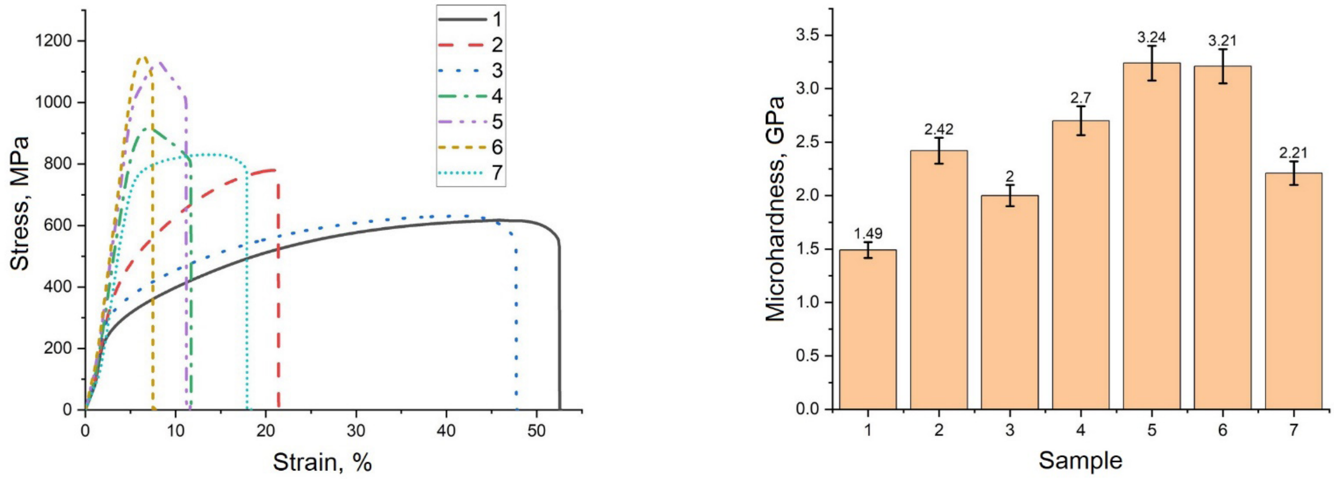

a *b*

Fig. 4. Tensile curves (a) and microhardness (b) of *Cu-9Al-2Mn* bronze samples

absolute maximum of $\boldsymbol{\sigma_{0.2}}$ = 1,095 MPa. After annealing at 500 °C for 10 minutes (sample 7), the bronze significantly softens and its plasticity is partially restored.

Thus, the change in the mechanical properties of the *Cu-9Al-2Mn* alloy is due to structural-phase evolution, changes in grain size, and defect density. The initial annealing of hot-rolled bars ensures high plasticity, while quenching for martensite increases strength due to internal stresses but reduces plasticity. Dispersion hardening after aging ensures a balance between strength and plasticity. Severe plastic deformation forms an ultrafine-grained structure, which, according to the *Hall–Petch* grain boundary strengthening mechanism, explains the hardening and loss of plasticity. As a result of polygonization and deformation aging occurring during annealing at 400 °C, dislocations form dense walls, and ultrafine precipitates pin them, leading to an anomalous increase in the yield strength. Recrystallization after annealing at 500 °C reduces strength but restores plasticity to 18%.

To assess the resistance to mechanical impact on the surface of *Cu-9Al-2Mn* alloy samples after various processing modes, scratch testing was performed. Analysis of scratches for samples 1–3 showed low resistance to surface deformation; however, the nature of the destruction in them is fundamentally different (Fig. 5).

The morphology of the scratch for sample 1 after annealing at 700 °C (Fig. 5,*a*) indicates the implementation of a mechanism of viscous plastic displacement of the metal to the periphery of the scratch (ploughing), where massive pile-ups of displaced metal are observed at the edges of the scratch and in front of the moving indenter. The high plasticity reserve ensures deformation without the formation of cracks or chips, which inevitably leads to a significant depth of indenter penetration of up to h = 13.3 μm (Fig. 6,*b*). After quenching at a temperature of 900 °C (sample 2), cracks are visible on the scratch surface (Fig. 5,*b*), and along its edges, there are individual heavily deformed grains with slip bands, while the gaps between them are free from deformation. Based on the structural characteristics, it can be considered that the grains of the α-phase are deformed, while the more brittle and harder martensitic phase is located in the gaps. Despite the mixed $\boldsymbol{\alpha} + \boldsymbol{\beta_1'} + \boldsymbol{\gamma_2}$ structure with increased strength and hardness, the maximum scratch depth increased to 14 μm. This may be related to the inability to undergo deformation hardening and low plasticity. As a result, the material fails under the loading by the indenter, which is confirmed by surface cracks. After aging (sample 3, Fig. 5,*c*), the maximum scratch depth remains at the same level (14.1 μm). The surface of the scratch does not contain noticeable cracks, which is consistent with the restored plasticity of the bronze and the reduction in the proportion of the brittle martensitic phase.

After *SPD*, the size of the scratches decreased sharply, and the deformation at their edges became more localized. After multi-axial forging (sample 4), local areas with adhered material are observed on the scratch surface (Fig. 5,*d*). This material detached from the scratch front due to its low plasticity and was pressed into the bronze surface by the indenter. At the edges of the scratch, the material was almost not deformed,

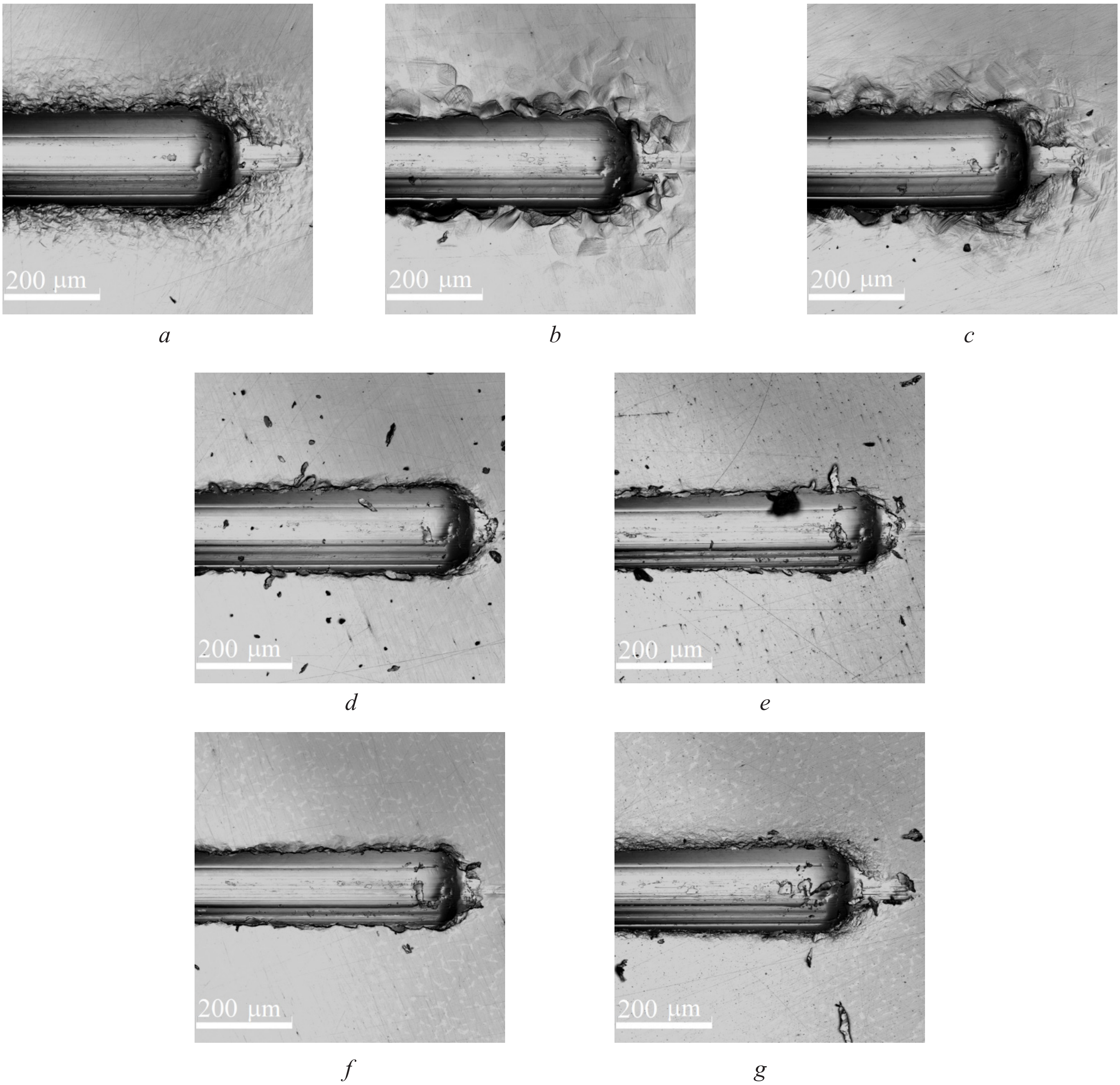

Fig. 5. Optical micrographs of scratches on *Cu-9Al-2Mn* bronze samples. Samples: 1 (*a*), 2 (*b*), 3 (*c*), 4 (*d*), 5 (*e*), 6 (*f*), and 7 (*g*)

which is consistent with the low plasticity of the material. The maximum scratch depth was 7.4 µm. After rolling (sample 5), the picture did not change significantly (Fig. 5,*e*). The scratch depth decreased to 6.9 µm. Otherwise, due to low plasticity and high microhardness, material adhesion to the scratch surface, chip formation at the edges of the scratch, and strong strain localization near the edges and in front of the indenter are maintained, which indicates a change in the mechanism from plastic displacement to micro-cutting with minimal plastic deformation.

Annealing at 400 °C for 30 minutes after rolling (sample 6) does not have a significant effect on the morphology of the surface and the edges of the scratch (Fig. 5,*f*), nor on the damage mechanism of the material. Microchips are also visible, material is sticking to the surface, and strong strain localization along the edges of the scratch is observed. The maximum depth of the scratch is 6.3 µm. Increasing the annealing temperature to 500 °C (sample 7) led to significant changes in the scratch morphology (Fig. 5,*g*). There is a partial return to the mechanism of elastic-plastic material deformation, which is visually confirmed by

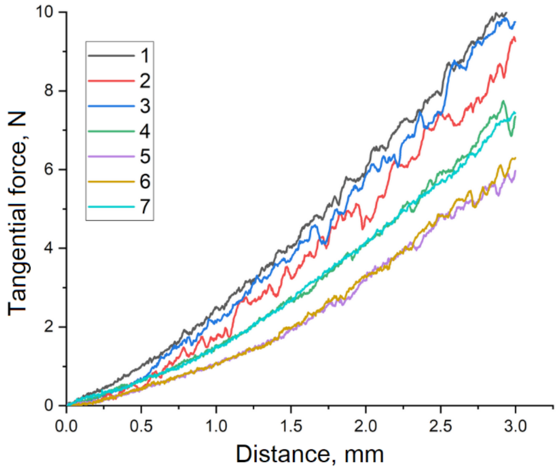

a

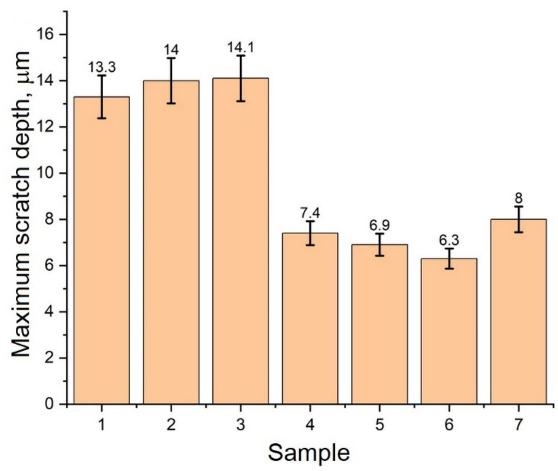

b

Fig. 6. Tangential force (*a*) during scratching and maximum scratch depth (*b*) for *Cu-9Al-2Mn* bronze samples

the resumption of the formation of wavy lateral bulges of the deformed material along the edges and the formation of a smooth plastic ridge in front of the indenter's tip. However, the microchips are also preserved. Therefore, the surface damage occurs through a combined mechanism of elastoplastic displacement with micro-cutting. The maximum scratch depth increased to 8 μm.

The graph of the change in tangential force (Fig. 6,*a*) as a function of scratch distance serves as a direct physical indication of the resistance force that the material exerts against the advancement of the diamond indenter. Since the normal load increases strictly linearly, the nature of the curves clearly shows how much energy is spent on elastoplastic displacement or micro-cutting during the scratching of samples with different structural-phase states. Based on the final values of shear force at a maximum load of 30 N, the samples are divided into three groups.

The first group, with the highest level of tangential force (~9.0–10.0 N), is formed from the initial coarse-grained states (samples 1–3). Due to the deep penetration of the indenter into the metal, the resistance to its movement increases significantly, and consequently, the tangential force also increases.

The second group consists of samples after multiaxial forging (sample 4) and after recrystallization annealing at 500 °C (sample 7). In the final section of the path, their tangential force stabilizes around ~7.0–7.5 N. In the case of sample 4, the reduction in shear force is associated with grain refinement and an increase in hardness, which decreases the scratch depth and, consequently, the volume of the deformed material. For sample 7, partial softening during recrystallization restores the material's plasticity, slightly increasing the scratch depth and resistance force compared to the sample after rolling. At the same time, the curves of the samples remain very smooth, indicating a uniform wear pattern without microcracks.

The third group is characterized by minimal values of tangential force ~6.0 N, recorded for samples 5 and 6 (rolling and subsequent low-temperature annealing at 400 °C). Their graphs almost merge over the entire scratching distance. This indicates that the ultrafine-grained structure after rolling and annealing possesses the highest surface strength. The indenter slides over the surface at a minimal depth, resulting in a nearly 40% reduction in tangential force compared to that of the initial annealing.

The results of tests under dry sliding friction conditions indicate a complex nature of the influence of the structural-phase state of the samples on their tribological properties. When analyzing the graphs of the change in the friction coefficient over the duration of the test (Fig. 7,*a*) and its average value (Fig. 7,*b*), no significant differences were found. From the moment sliding begins, the coefficient of friction (*COF*) slightly increases, which is due to the running-in of the friction pair. Then the *COF* stabilizes. On average, the *COF* varies from 0.21 to 0.23 with a range of values around 0.03.

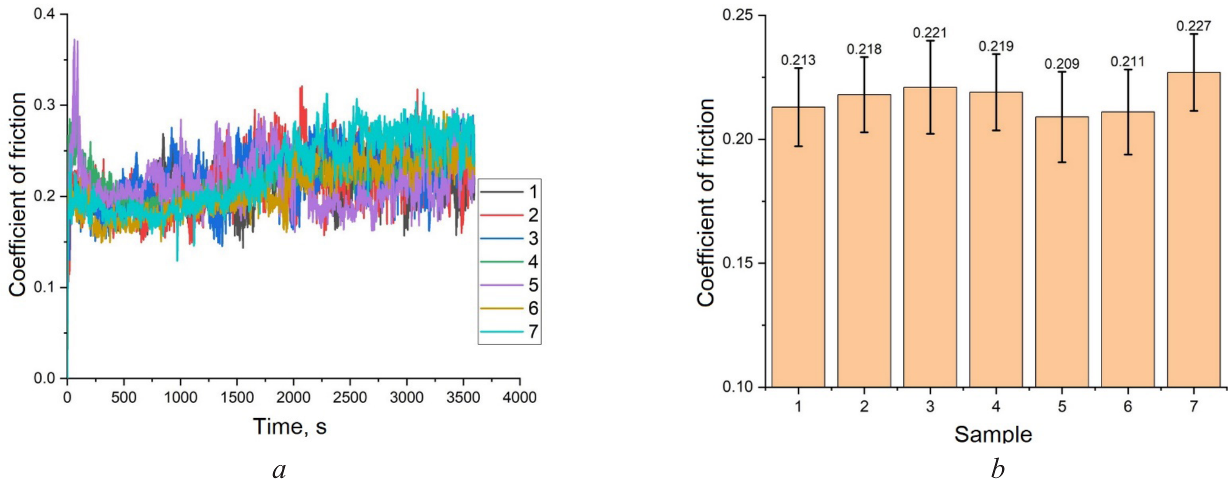

Fig. 7. Friction coefficient as a function of time in sliding tests (*a*) and its average values (*b*)

Based on the analysis of data on the wear track cross-sectional area (Fig. 8,*a*), vibrometry (Fig. 8,*b*), and acoustic emission (Fig. 8,*c–d*), it is possible to identify wear characteristics depending on the structural-phase state of the bronze.

Samples with a coarse-grained structure are characterized by low wear resistance. The maximum wear and highest vibration were recorded in the hot-rolled rod annealed at 700 °C (sample 1). At the same time, a high median frequency and acoustic emission (*AE*) energy are also recorded. The energy increases due to the rise in vibration, which results in more frequent collisions between the surfaces of the sample and the counterbody, causing elastic waves [24]. The high median frequency is due to the fact that during the

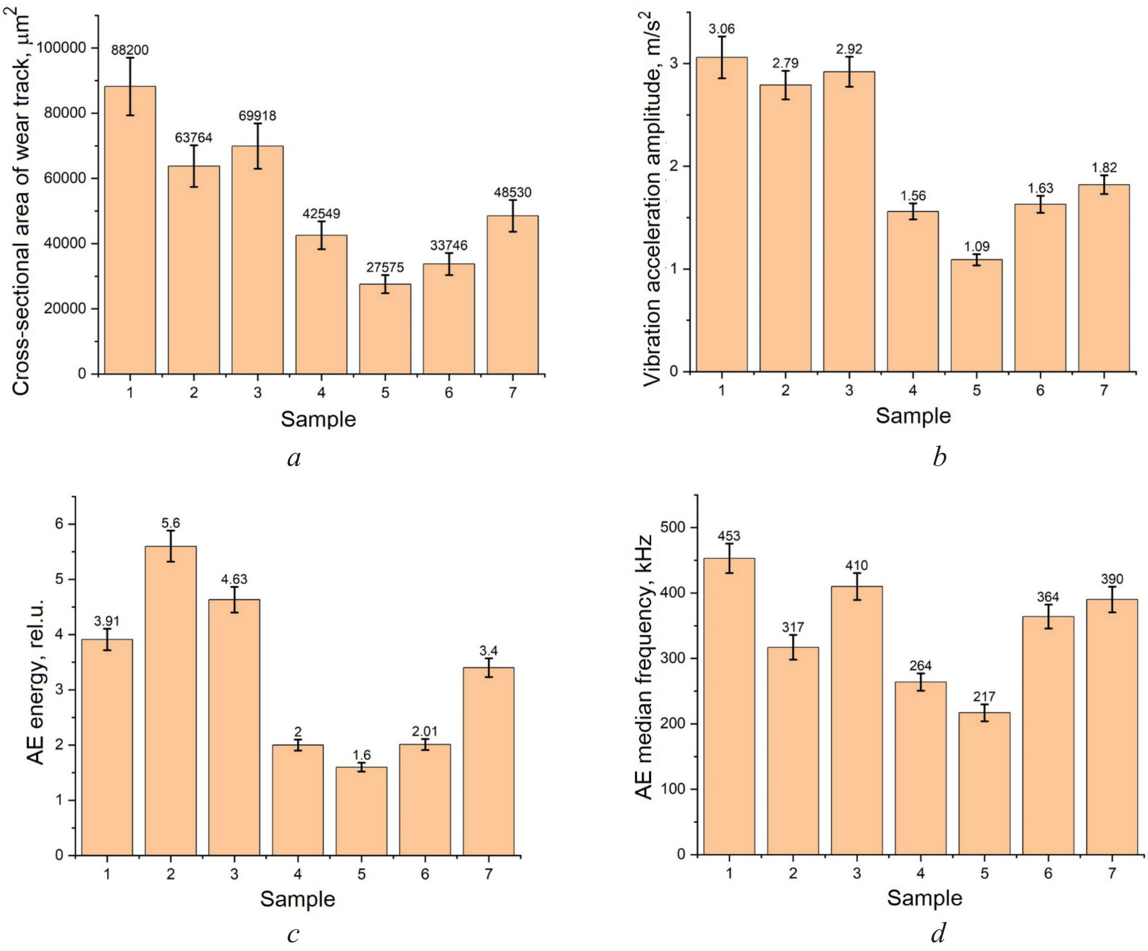

Fig. 8. Mean cross-sectional area of wear tracks (*a*), vibration acceleration amplitude (*b*), *AE* energy (*c*) and *AE* median frequency (*d*) during tribological tests

friction of plastic bronze, elastoplastic deformation and viscous destruction of microcontact spots prevail, which is consistent with previously conducted work [16]. After quenching at a temperature of 900 °C (sample 2), wear decreases, which is due to the increase in the strength and hardness of the material. Vibration decreases, but not significantly. The high energy and low median frequency of *AE* are apparently associated with the quasi-brittle fracture of martensite during the friction process. Subsequent aging at 400 °C (sample 3) partially restores plasticity, reducing *AE* energy and increasing the median frequency due to a return to viscous shear. As a result, it can be concluded that the reduction in mechanical properties led to increased wear.

The refinement of the structure by severe plastic deformation fundamentally changes the tribological characteristics of the studied bronze. Multiaxial forging (sample 4) significantly reduces the wear rate. Vibrations, median frequency, and *AE* energy are also reduced compared to the coarse-grained samples 1–3. This confirms the change in wear conditions and the transition to more stable friction. After rolling (sample 5), wear decreases to a minimum value. Vibrations and *AE* signal parameters have also decreased. The decrease in median frequency in samples after *SPD* indicates that large-scale plastic shifts are blocked in the material, and that deformation is localized in a thin near-surface layer. This also leads to a change in the mechanism of destruction of adhesive bonds in the microcontact from ductile to brittle fracture.

Subsequent low-temperature annealing at 400 °C (sample 6) leads to a slight increase in wear. In this case, the median frequency of *AE* sharply increases. This is consistent with the processes of polygonization and deformation aging. As a result, the likelihood of dislocation formation, as one of the sources of *AE*, increases. Ten minutes of holding the sample at a temperature of 500 °C (sample 7) was sufficient to activate primary recrystallization and grain growth to 200–500 nm. The reduction in strength and microhardness, as well as the low density of crystal lattice defects, cause the material to be easier to deform again. The median frequency increases due to the increase in the share of elastoplastic deformation of the bronze. The energy of *AE* and vibrations increases due to the formation of a greater number of wear particles during the intensification of the latter.

The morphology of the wear track of coarse-grained bronze annealed at 700 °C (sample 1) indicates the development of intense adhesive wear with oxidation (Fig. 9,*a*). Deep, clearly oriented longitudinal grooves are formed on the surface, accompanied by the formation of massive ragged accumulations of forced-out metal along the periphery of the track. The presence of dark dispersed areas at the bottom of the grooves indicates the occurrence of tribooxidation and cyclic adhesive material transfer [25]. After quenching from a temperature of 900 °C (sample 2), the morphology of the wear track does not change (Fig. 9,*b*), but the intensity of material displacement to the periphery of the track decreases. After aging at 400 °C (sample 3), no torn protrusions on the periphery are observed, dark oxidation spots occupy a larger area, and traces of adhesive material transfer are more distinctly observed (Fig. 9,*c*).

After multi-axial forging (sample 4), a qualitative change in the nature of surface frictional destruction is observed. The slip lines are slightly curved, and the fragments of material adhering to the surface as a result of adhesive transfer have significantly increased (Fig. 9,*g*). No accumulations of plastically displaced material are observed. Rolling (sample 5) resulted in the complete absence of edge pile-ups (Fig. 9,*d*). Oxides and traces of reverse adhesive material transfers are more evenly distributed across the surface; the grooves are still curved, but to a lesser extent.

Low-temperature annealing at 400 °C after rolling (sample 6) led to an intensification of adhesion transfer and oxidation processes (Fig. 9,*e*). On the surface of the track, the oxide layer is the thickest and it can serve as an effective wear protection. Lateral protrusions are observed only on the outer radius of the wear track. Increasing the annealing temperature to 500 °C (sample 7) had almost no effect on the wear track surface morphology (Fig. 9,*g*), compared to sample 5.

On the surface of the balls after sliding in a pair with bronze annealed at 700 °C (sample 1), rough longitudinal grooves and pronounced dark zones are visible (Fig. 10,*a*). The contact spot has an elliptical shape. This indicates intense adhesive bonding with bronze, accompanied by sticking and frictional oxidation. A similar morphology was observed on the balls after rubbing against sample 3 (quenching at

Fig. 9. Optical micrographs of the wear track surfaces of *Cu-9Al-2Mn* bronze samples. Samples: 1 (*a*), 2 (*b*), 3 (*c*), 4 (*d*), 5 (*e*), 6 (*f*), and 7 (*g*)

900 °C and aging at 400 °C). After sliding in a pair with hardened bronze (sample 2), the contact spot has a more elongated shape; the oxides are dark and cover the contact spot more evenly (Fig. 10,*b*).

The characteristic appearance of the ball counterpart surface after sliding in pairs with samples subjected to multi-axial forging (sample 4) and rolling (sample 5) indicates that the oxide layer is distributed very

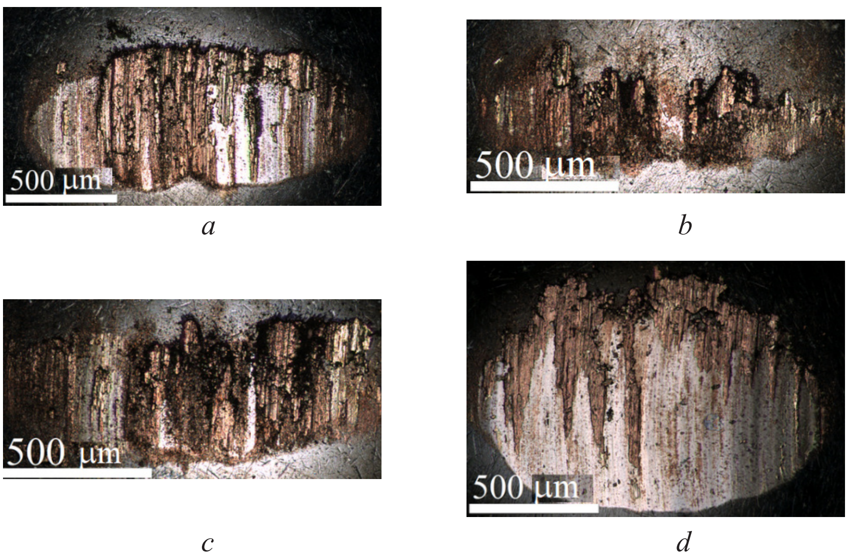

Fig. 10. Optical micrographs of the steel ball surfaces after sliding against *Cu-9Al-2Mn* bronze samples. Samples: 1, 3 (*a*), 2 (*b*), 4–5 (*c*), and 6–7 (*d*)

uniformly in the form of a dense dark film of adhered material (Fig. 10,*c*), which is an oxidized mechanical mixture of the soft phase of copper and wear particles. When bronze is subjected to sliding after annealing at 400 °C (sample 6) and 500 °C (sample 7), a wide smooth contact spot forms on the surface of the balls. The adhered material is concentrated on the frontal part of the contact spot (Fig. 10,*d*).

The study of metallographic images of longitudinal sections in the contact zone allowed the examination of the nature of plastic deformation occurring in the subsurface layers of the *Cu-9Al-2Mn* alloy after sliding (Fig. 11). Sliding without lubrication causes the formation of a pronounced deformation gradient, the direction and depth of which are determined by the structural-phase state of the samples.

Under the worn surface of bronze annealed at 700 °C (sample 1), the large grains of the **α**-phase at the very edge of the track are strongly elongated along the direction of the counterbody's movement (Fig. 11,*a*). The dark inclusions are fragmented and mechanically mixed with the matrix, forming a highly deformed layer on the surface. After quenching from 900 °C (sample 2), the deformation is localized in a thin near-

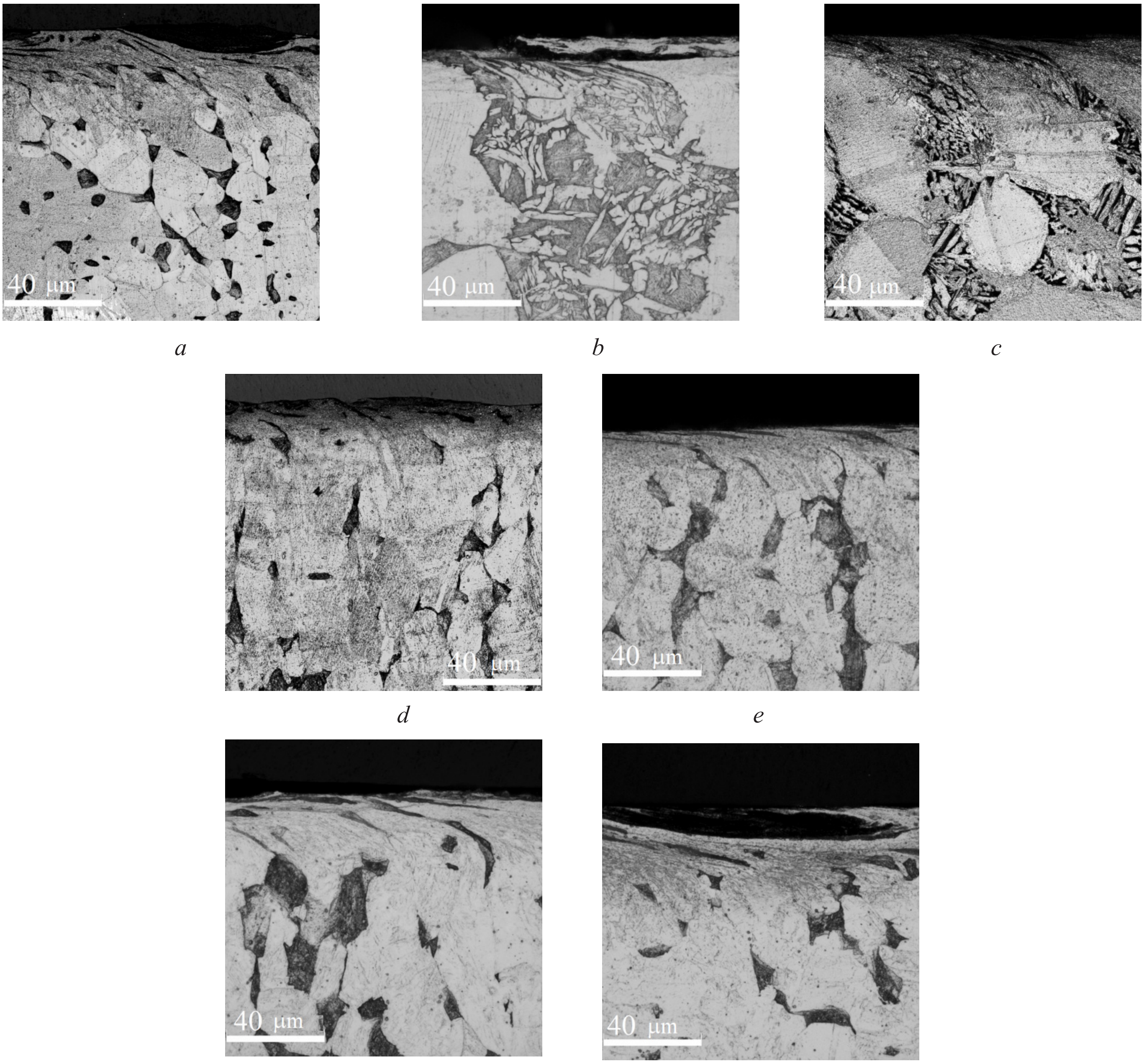

a *b* *c* *d* *e* *f* *g*

Fig. 11. Optical micrographs of the subsurface microstructure of *Cu-9Al-2Mn* bronze beneath the wear track surface. Samples:
1 (*a*), 2 (*b*), 3 (*c*), 4 (*d*), 5 (*e*), 6 (*f*), and 7 (*g*)

surface layer with a thickness of 15–20 μm (Fig. 11,*b*). Emerging microcracks parallel to the surface are visible, confirming the martensitic structure's tendency toward brittle failure. Aging after quenching (sample 3) leads to a repetition of the deformation pattern of sample 1. The grains of the ductile α-phase are elongated along the direction of the friction force, followed by the β' and γ_2 phases being involved in the deformation (Fig. 11,*c*).

For samples 4 and 5, which underwent severe plastic deformation via multiaxial forging (Fig. 11,*g*) and rolling (Fig. 11,*d*), the characteristic feature is the almost complete suppression of plastic deformation. The photographs capture a smooth, flat wear track surface without macroscopic scratches and tears. Due to strong hardening, the depth of the shear zone is localized in the thinnest surface layer (~5–10 μm). There is no large-scale distortion or rotation of the underlying grains. This indicates a high resistance of the formed *SPD* structure to shear deformation.

Low-temperature annealing at 400 °C (sample 6) resulted in a more pronounced plastic shear in the near-surface layer of the bronze (Fig. 11,*e*). A thin but the most uniform layer of oxidized mechanical mixture of soft bronze and wear particles forms near the surface.

After annealing at 500 °C (sample 7), there is a significant reduction in shear resistance, which is caused by recrystallization and a decrease in the degree of cold work. Due to the appearance of defect-free nanograins (200–500 nm) and the overall softening of the material at the edge of the wear track, the nature of the quasi-viscous flow of the material is clearly visible (Fig. 11,*f*). The edge of the contact becomes uneven, and the surface layer contains areas of oxidized mechanical mixture of soft bronze and wear particles.

Conclusions

In this work, a comprehensive study of the evolution of the structural-phase state, mechanical, and tribological properties of aluminum bronze *Cu-9Al-2Mn* under various heat treatment conditions, severe plastic deformation (*SPD*), and subsequent low-temperature annealing was conducted. Based on the obtained data, the following main conclusions have been formulated:

It has been established that severe plastic deformation by multi-axial forging followed by rolling at room temperature forms an ultrafine-grained structure (100–300 nm) in *Cu-9Al-2Mn* bronze, strengthened by deformation-induced martensite, twinning, and a high dislocation density. Low-temperature annealing at 400 °C causes polygonization and the precipitation of γ_2-phase particles, while annealing at 500 °C leads to primary recrystallization with the formation of equiaxed grains of 300–700 nm.

According to mechanical tests, it has been found that *SPD* increases the yield strength by approximately 2.5 times (up to 998 MPa) and the microhardness to 3.24 GPa, while reducing plasticity, compared to hot-rolled bars after annealing. Annealing at 400 °C further increases the yield strength to 1,095 MPa due to the grain boundary strengthening mechanism. Recrystallization at 500 °C reduces strength but restores plasticity to ~18%.

It has been established that samples after *SPD* resist scratching damage better, as confirmed by the minimal scratch depth and a 40% reduction in tangential force compared to coarse-grained samples. The failure mechanism changes from ductile penetration to elastic-plastic displacement with micro-cutting; surface cracks and massive bulges disappear.

Based on the results of dry sliding testing, it has been found that the friction coefficient is almost independent of the structural-phase state of the samples. *SPD* significantly increases wear resistance compared to thermally treated coarse-grained samples. After annealing at 500 °C, wear increases but remains lower than in coarse-grained states. According to the results of metallographic studies, it has been established that during friction in coarse-grained samples with high plasticity, plastic flow of the material in the direction of friction is observed. After quenching at 900 °C, the deformation is localized in a thin surface layer 15–20 μm thick, resulting in the formation of microcracks. Due to strong hardening, the depth of the shear zone in the samples after *SPD* is localized in a surface layer approximately 5–10 μm thick.

Based on the vibrometry and *AE* data, it was established that during the sliding of coarse-grained samples, the vibrations of the tribosystem are the most intensive. High values of energy and median frequency of *AE* are due to the viscous nature of the adhesive bonds at micro-asperities. When transitioning to more brittle failure and the formation of subsurface microcracks, there is a decrease in median frequency due to the shift of deformation and failure to a higher scale level.

The obtained results open up broad prospects for the use of aluminum bronze *Cu-9Al-2Mn* in an ultrafine-grained modified state for the manufacture of highly loaded friction units, sliding bearings, heavily loaded worm pairs, and valve components operating under harsh conditions of dry sliding and abrasive wear.

As directions for further research, it is proposed to study the thermal stability of the ultrafine structure during prolonged heating, to conduct tribological tests in aggressive environments and under abrasive wear, as well as to assess cyclic fatigue strength.

References

1. Shangina D.V., Gubicza J., Dodony E., Bochvar N.R., Straumal P.B., Tabachkova N.Yu., Dobatkin S.V. Improvement of strength and conductivity in Cu-alloys with the application of high pressure torsion and subsequent heat-treatments. *Journal of Materials Science*, 2014, vol. 49, pp. 6674–6681. DOI: 10.1007/s10853-014-8339-4.

2. Qu S., An X.H., Yang H.J., Huang C.X., Yang G., Zang Q.S., Wang Z.G., Wu S.D., Zhang Z.F. Microstructural evolution and mechanical properties of Cu–Al alloys subjected to equal channel angular pressing. *Acta Materialia*, 2009, vol. 57 (5), pp. 1586–1601. DOI: 10.1016/j.actamat.2008.12.002.

3. Valiev R.Z., Islamgaliev R.K., Alexandrov I.V. Bulk nanostructured materials from severe plastic deformation. *Progress in Materials Science*, 2000, vol. 45, pp. 103–189. DOI: 10.1016/S0079-6425(99)00007-9.

4. Osintsev O.E., Fedorov V.N. *Med' i mednye splavy. Otechestvennye i zarubezhnye marki* [Copper and copper alloys. domestic and foreign brands]. Reference book. 2nd ed. rev. Moscow, Innovatsionnoe mashinostroenie Publ., 2016. 360 p. ISBN 978-5-9907638-3-8.

5. Kroupa A., Zobač O., Richter K.W. The thermodynamic reassessment of the binary Al–Cu system. *Journal of Materials Science*, 2021, vol. 56, pp. 3430–3443. DOI: 10.1007/s10853-020-05423-7.

6. Zobac O., Kroupa A., Zemanova A., Richter K.W. Experimental вescription of the Al–Cu binary phase diagram. *Metallurgical and Materials Transactions A*, 2019, vol. 50, pp. 3805–3815. DOI: 10.1007/s11661-019-05286-x.

7. Alés A. Study of different structures derives of β-Cu_3Al by means of ab-initio calculations and quasi-harmonic approximation. *Computational Condensed Matter*, 2022, vol. 31, p. e00652. DOI: 10.1016/j.cocom.2022.e00652.

8. Huang R., Zhu D., Liao X., Yan Q. Effect of ECAP process and subsequent annealing on microstructure and properties of Cu–0.25Se–0.25Te alloy. *Journal of Electronic Materials*, 2020, vol. 49, pp. 2617–2624. DOI: 10.1007/s11664-020-07975-5.

9. Hase A., Mishina H., Wada M. Correlation between features of acoustic emission signals and mechanical wear mechanisms. *Wear*, 2012, vol. 292–293, pp. 144–150. DOI: 10.1016/j.wear.2012.05.019.

10. Towsyfyan H., Gu F., Ball A.D., Liang B. Tribological behaviour diagnostic and fault detection of mechanical seals based on acoustic emission measurements. *Friction*, 2019, vol. 7, pp. 572–586. DOI: 10.1007/s40544-018-0244-4.

11. Hase A., Mishina H. Identification and evaluation of wear phenomena under electric current by using an acoustic emission technique. *Tribology International*, 2018, vol. 127, pp. 372–378. DOI: 10.1016/j.triboint.2018.06.027.

12. Kolubaev E.A., Kolubaev A.V., Sizova O.V. Analysis of acoustic emission during sliding friction of manganese steel. *Technical Physics Letters*, 2010, vol. 36 (8), pp. 762–765. DOI: 10.1134/S1063785010080250.

13. Rubtsov V.E., Kolubaev E.A., Kolubaev A.V., Popov V.L. Using acoustic emission for the analysis of wear processes during sliding friction. *Technical Physics Letters*, 2013, vol. 39 (2), pp. 223–225. DOI: 10.1134/S1063785013020235.

14. Filippov A.V., Tarasov S.Yu., Fortuna S.V., Podgornykh O.A., Shamarin N.N., Rubtsov V.E. Microstructural, mechanical and acoustic emission-assisted wear characterization of equal channel angular pressed (ECAP) low stacking fault energy brass. *Tribology International*, 2018, vol. 123, pp. 273–285. DOI: 10.1016/j.triboint.2018.03.023.

15. Filippov A.V., Tarasov S.Y., Podgornykh O.A., Fortuna S.V., Shamarin N.N., Vorontsov A.V. Wear, vibration and acoustic emission characterization of sliding friction processes of coarse-grained and ultrafine-grained copper. *Wear*, 2019, vol. 424–425, pp. 78–88. DOI: 10.1016/j.wear.2019.02.014.

16. Filippov A.V., Rubtsov V.E., Tarasov S.Y. Acoustic emission study of surface deterioration in sliding steel contacts. *Applied Acoustics*, 2017, vol. 117, pp. 106–112. DOI: 10.1016/j.apacoust.2016.11.007.

17. Deng Z., Yin H., Zhang C., Zhang G., Zhang T., Liu Z., Wang H., Qu X. Sintering mechanism of Cu–9Al alloy prepared from elemental powders. *Progress in Natural Science: Materials International*, 2019, vol. 29 (4), pp. 425–431. DOI: 10.1016/j.pnsc.2019.04.007.

18. Kainuma R., Satoh N., Liu X.J., Ohnuma I., Ishida K. Phase equilibria and Heusler phase stability in the Cu-rich portion of the Cu–Al–Mn system. *Journal of Alloys and Compounds*, 1998, vol. 266 (1-2), pp. 191–200. DOI: 10.1016/S0925-8388(97)00425-8.

19. Zykova A., Panfilov A., Chumaevskii A., Vorontsov A., Gurianov D., Savchenko N., Kolubaev E., Tarasov S. Decomposition of β′-martensite in annealing the additively manufactured aluminum bronze. *Materials Letters*, 2023, vol. 338, p. 134064. DOI: 10.1016/j.matlet.2023.134064.

20. Ge Y., Vronka M., Veřtát P., Karlik M., Hannula S.P., Heczko O. Deformation twinning with different twin-boundary mobility in 2H martensite in Cu–Ni–Al shape memory alloy. *Acta Materialia*, 2022, vol. 226, p. 117598. DOI: 10.1016/j.actamat.2021.117598.

21. Sedlák P., Seiner H., Landa M., Novák V., Šittner P., Mañosa L. Elastic constants of bcc austenite and 2H orthorhombic martensite in CuAlNi shape memory alloy. *Acta Materialia*, 2005, vol. 53, pp. 3643–3661. DOI: 10.1016/j.actamat.2005.04.013.

22. Liverić L., Sitek W., Snopiński P., Maziarz W., Grgurić T.H. A microstructural study of Cu–10Al–7Ag shape memory alloy in as-cast and quenched conditions. *Symmetry*, 2024, vol. 16, p. 545. DOI: 10.3390/sym16050545.

23. Han Z., Zhao H. Effect of β martensite transformation on dealuminification behavior of Cu–9Al–2Mn alloy in a marine environment. *Materials Science and Engineering A*, 2003, vol. 345, pp. 8–13. DOI: 10.1016/S0921-5093(02)00124-7.

24. Olejnik P., Desta Y.D. Friction-induced interactions: acoustic emissions, vibrations, and wear – a multiscale review. *Nonlinear Dynamics*, 2025, vol. 113, pp. 24101–24140. DOI: 10.1007/s11071-025-11397-5.

25. Tarasov S.Yu., Filippov A.V., Kolubaev E.A., Kalashnikova T.A. Adhesion transfer in sliding a steel ball against an aluminum alloy. *Tribology International*, 2017, vol. 115, pp. 191–198. DOI: 10.1016/j.triboint.2017.05.039.

Conflicts of Interest

The authors declare no conflict of interest.